J. Fluid Mech. (1987), *vol.* 180, *pp.* 327–342
Printed in Great Britain

The role of the buoyancy layer in determining the structure of salt fingers

By GEORGE VERONIS
Department of Geology and Geophysics, Yale University, New Haven, CT 06511, USA

(Received 15 May 1986 and in revised form 15 October 1986)

An initial state consisting of sugar solution lying above a denser salt solution in a Hele-Shaw cell is unstable to disturbances that evolve into long, slender fingers. An analysis of the structure of fully evolved (infinitely long) fingers that are independent of the vertical coordinate concludes that fingers with a width of the order of the buoyancy-layer thickness have maximum growth rate. Since effective gravity can be altered by inclining the Hele-Shaw cell toward the horizontal, fingers of different preferred widths can be established. An abrupt change of the angle of inclination changes the preferred width. A stability analysis of the resulting initial-value problem shows that perturbations with a vertical scale of the order of the buoyancy-layer thickness grow, and fluid from each finger penetrates laterally into the two adjacent fingers. The unstable modes resemble those observed experimentally by Taylor & Veronis (1986). It turns out that all vertically uniform fingers, even ones with the preferred width of the basic state, are unstable to a non-oscillatory peturbation that changes straight fingers to ones that have a vertically wavy structure. In all cases the vertical scale of the most unstable disturbance is of the order of the buoyancy-layer thickness. Also included is a discussion of the need for a model describing the transient evolution of fingers and particularly one that contains an analysis of the role of the transition region between the salt-finger zone and the reservoirs above and below.

1. Introduction

In describing a series of experiments to study the evolution of salt fingers in a Hele-Shaw cell, Taylor & Veronis (1986) reported several features that have received little or no attention in the past. An initially two-layer configuration with a sugar solution lying above a slightly denser salt solution becomes unstable to a disturbance that evolves rapidly into an array of very narrow fingers. The growing length of the fingers is accompanied by a reduction of the mean salt and sugar gradients near the interface and a concomitant increase in the preferred finger width of the individual cells. The increase in width appears to be generated by the growth of fingers in the transition region between the finger zone and the reservoirs, where the mean stabilizing (salt) gradient is smaller and wider fingers are preferred. These wide fingers penetrate from the transition region into the finger zone, 'swallowing' narrower fingers along the way. The wider fingers are in turn replaced by even wider ones as the evolution continues.

The phenomenon just described appeared to continue during the lifetime of the experiment even when the finger zone occupied essentially the entire depth of the tank. Evidently, as the reservoirs disappear and the system runs down, the mean gradients continue to decrease and to support ever wider fingers which always seem

to penetrate in from the outer edges of the finger zone. The right-hand side of figure 3(*a*) shows a late stage in the evolution with interpenetrating fingers from above and below reflecting an unsettled state in one part of the experiment while a more uniform pattern of fingers existed in the left-hand part.

The same gross behaviour can be expected for fingers in a regular fluid where the property distributions differ in detail from those of the Hele-Shaw cell but which should not affect the overall evolution of the system. However, the Hele-Shaw configuration does provide a control that is not possible with a a regular fluid. Tilting the experiment so that the plates are inclined at an angle θ ($< 90°$) to the horizontal reduces the effect of gravity and changes the preferred width of the fingers. Thus, one can generate a finger pattern with θ at a given value and then abruptly change θ so that a different scale is preferred. The adjustment of the system to a different value of effective gravity can be treated as an initial-value problem in which one examines the stability of the established pattern. This affords an analysis of the mechanism of instability that can be verified experimentally.

The present study begins with a description of infinitely long fingers with a sinusoidal, horizontal distribution of properties and with vertically uniform gradients of salt and sugar. There is an infinite amount of potential energy available in the destabilizing sugar gradient. A specific finger width corresponds to steady-state equilibrium, but wider fingers grow exponentially in time and one particular width gives rise to maximum growth rate.

These results are very similar to what one derives for a regular fluid (Stern 1969), but the buoyancy-layer scale, which characterizes the horizontal structure, is different. The buoyancy-layer scale can be described as the intrinsic scale that emerges from the linear balances obtained from the vertical momentum equation and the diffusion equation when the perturbations depend only on the horizontal coordinate x. Thus, take

$$\mu w = g\alpha T,$$

$$w\overline{T}_z = \kappa_T \frac{\partial^2 T}{\partial x^2},$$

where μ, the Darcy coefficient of momentum dissipation, replaces the usual viscous term, $-\nu\,\partial^2/\partial x^2$. Eliminating T yields

$$\frac{\partial^2 w}{\partial x^2} = \frac{g\alpha\overline{T}_z}{\mu\kappa_T} w,$$

and the buoyancy-layer scale, $(\mu\kappa_T/g\alpha\overline{T}_z)^{\frac{1}{2}}$, emerges. In a regular fluid it is $(4\nu\kappa_T/g\alpha\overline{T}_z)^{\frac{1}{4}}$ (Howard & Veronis 1987).

The buoyancy-layer scale determines the horizontal distance required to adjust property differences across finger boundaries. The horizontal scale for equilibrium fingers and for those with maximum growth rate are proportional to the buoyancy-layer scale. Of particular interest in the present problem is the fact that this scale varies as $g^{-\frac{1}{2}}$. Thus, when effective gravity ($g \sin\theta$) is small, the scale is large, and vice versa.

When the Hele-Shaw cell is inclined so that θ is small, wide cells are generated. After these have been established, the apparatus can be raised upright so that the property difference across a finger boundary is adjusted in the narrower region of the reduced buoyancy-layer scale. Thus, thin boundary layers are generated on both sides of each finger boundary. When that boundary layer is perturbed by a disturbance with a vertical lengthscale of the order of the buoyancy-layer scale, the disturbance

grows and penetrates into the relatively uniform interior of the finger. Taylor & Veronis (1986) carried out an experiment following the procedure just described and recorded the evolved instability shown in figure 3(*b*). The stability analysis for the system is outlined in §3 and application to the stability of wide fingers is described in §4. The results support the qualitative description offered by Taylor & Veronis (1986) and summarized in §4.

The instability just described develops because the established finger pattern is not consistent with the new conditions of the system. But one can also enquire into the stability of fingers with the 'preferred' scale, the one corresponding to maximum growth rate. If the latter become unstable, then the system will seek a configuration other than that of infinitely long fingers with sinusoidal, horizontal structure. In that case, long straight fingers will not be observed even though they are exact solutions to the equations with the prescribed periodicity.

Since the fingers with maximum growth rate are not steady, a rigorous stability analysis is not simple. However, if one explores the stability assuming that the basic fingers are quasi-steady and if the derived growth rate of the instability is much larger than that of the basic finger itself, the results will have meaning. That forms the basis for the calculations of §4.2 which show that long straight fingers are always unstable to a non-oscillating perturbation with a vertical lengthscale roughly that of the buoyancy-layer thickness. Both the rationale and the mathematical procedure are the same as Holyer (1984) used to come to the same conclusion about the stability of steady, long fingers in a regular fluid.

The last case analysed here is one in which a pattern of thin fingers is established and then the apparatus is inclined toward the horizontal so that gravity is halved and slightly wider fingers are preferred. This system is also unstable to a non-oscillatory perturbation with a vertical lengthscale determined by the buoyancy-layer thickness.

Qualitatively, the instability that occurs in all of the cases appears to be independent of the initial horizontal scale of the fingers. The finite-amplitude evolution of the perturbation is likely to vary as a function of the scale of the initial fingers, but that lies outside the scope of the present theory. Because the momentum balance in a Hele-Shaw cell is between buoyancy, pressure gradients and Darcy friction, inertial terms play no role in the instability. Consequently, the collective instability of Stern (1969) and Holyer (1981, 1984) is not obtained here.

The article ends with speculation about the applicability of this approach to the actual physical system and with some qualitative conclusions based on the analysis and on the experiments.

2. Fully developed fingers

In an infinite system with horizontally averaged gradients of T and S and with the Hele-Shaw form of viscous dissipation the Boussinesq equations take the form

$$\mu \boldsymbol{v} = -\nabla P + g(\alpha T - \beta S)\,\hat{\boldsymbol{k}}, \tag{2.1}$$

$$\nabla \cdot \boldsymbol{v} = 0, \tag{2.2}$$

$$T_t + \boldsymbol{v} \cdot \nabla T + w\overline{T}_z = \kappa_T \nabla^2 T, \tag{2.3}$$

$$S_t + \boldsymbol{v} \cdot \nabla S + w\overline{S}_z = \kappa_S \nabla^2 S, \tag{2.4}$$

where μ ($= 12\nu/d^2$: ν is the kinematic viscosity and d is the gap width between the plates) is the Darcy drag coefficient, P is the pressure divided by (constant) density, $\hat{\boldsymbol{k}}$ is the unit vertical vector and κ_T and κ_S are the diffusion coefficients of T and S respectively, with $\kappa_S < \kappa_T$. The variable density in the buoyancy term is taken to be a linear function of T and S,

$$\frac{\rho}{\rho_0} = 1 - \alpha T + \beta S, \tag{2.5}$$

where $\alpha = -(1/\rho_0)(\partial\rho/\partial T)$, $\beta = (1/\rho_0)(\partial\rho/\partial S)$. (The negative sign for αT is appropriate for temperature. This notation is retained even though the application in this article is to sugar and salt. With the present notation sugar would be represented by S and salt by $-T$.) The horizontally averaged gradients of T and S are written separately as $\overline{T}_z$ and $\overline{S}_z$ and subscripts t and z refer to partial derivatives.

A vertically infinite system with constant mean gradients and z-independent variables takes the simpler (exact) form

$$\mu w = g(\alpha T - \beta S), \tag{2.6}$$

$$T_t + w\overline{T}_z = \kappa_T T_{xx}, \tag{2.7}$$

$$S_t + w\overline{S}_z = \kappa_S S_{xx}, \tag{2.8}$$

where the hydrostatic pressure balance has been subtracted from (2.6). This system has solutions that are periodic in x and exponential in t,

$$(w, \alpha T, \beta S) = (\hat{w}, -\hat{T}, -\hat{S})\, e^{\lambda_* t} \sin l_* x, \tag{2.9}$$

where $\hat{w}, \hat{T}, \hat{S}$ must satisfy

$$\mu\hat{w} = -g(\hat{T} - \hat{S}), \tag{2.10}$$

$$(\lambda_* + \kappa_T l_*^2)\hat{T} = \hat{w}\alpha\overline{T}_z, \tag{2.11}$$

$$(\lambda_* + \kappa_S l_*^2)\hat{S} = \hat{w}\beta\overline{S}_z. \tag{2.12}$$

Equations (2.10) to (2.12) lead to a dispersion relation between λ_* and l_*. However, for closer contact with the physics of the system (particularly for comparison with experiments) it is convenient to introduce the buoyancy flux ratio as an intermediate dependent variable (Schmitt 1979).

Take

$$\langle w\alpha T\rangle \equiv \int_{-\pi/l_*}^{\pi/l_*} \frac{-\hat{w}\hat{T}\sin^2 l_* x\, e^{2\lambda_* t}\, dx}{2\pi/l_*} = -\tfrac{1}{2}\hat{w}\hat{T}\, e^{2\lambda_* t}, \tag{2.13}$$

$$\langle w\beta S\rangle = -\tfrac{1}{2}\hat{w}\hat{S}\, e^{2\lambda_* t}, \tag{2.14}$$

and define the buoyancy flux ratio

$$F_r = \frac{\langle \alpha w T\rangle}{\langle \beta w S\rangle} = \frac{\hat{T}}{\hat{S}}. \tag{2.15}$$

Then (2.10) becomes

$$\hat{w} = \frac{g\hat{S}}{\mu}(1 - F_r) = \frac{g\hat{T}}{\mu}\left(\frac{1 - F_r}{F_r}\right). \tag{2.16}$$

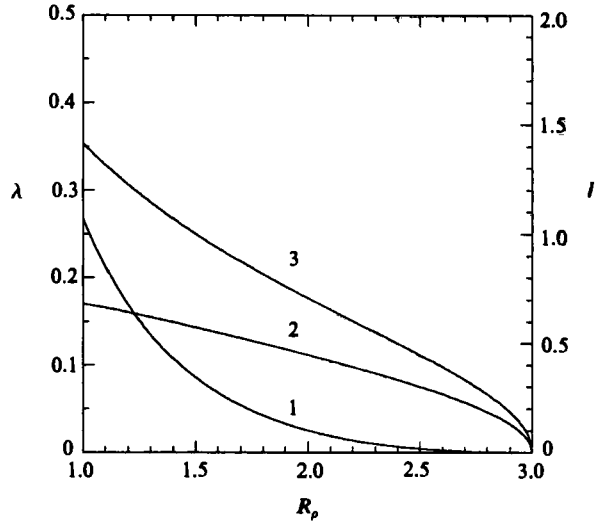

FIGURE 1. Plots of λ (curve 1), l_m (curve 2) and l_e (curve 3) *vs.* R_ρ for infinitely long sugar–salt fingers with no vertical structure.

Use of (2.11) and (2.12) yields

$$\lambda + l^2 = \frac{1-F_r}{F_r}, \quad l^2 = \frac{l_*^2 \mu \kappa_T}{g\alpha \overline{T}_z}, \quad \lambda = \frac{\lambda_* \mu}{g\alpha \overline{T}_z}, \tag{2.17}$$

$$\lambda + \tau l^2 = \frac{1-F_r}{R_\rho}, \tag{2.18}$$

where

$$\tau = \frac{\kappa_S}{\kappa_T}, \quad R_\rho = \frac{\alpha \overline{T}_z}{\beta \overline{S}_z}. \tag{2.19}$$

Then l^2 and λ can be evaluated as

$$l^2 = \frac{1-F_r}{1-\tau}\left(\frac{1}{F_r} - \frac{1}{R_\rho}\right), \tag{2.20}$$

$$\lambda = \frac{1-F_r}{1-\tau}\left(\frac{1}{R_\rho} - \frac{\tau}{F_r}\right). \tag{2.21}$$

The growth rate vanishes at $F_r = \tau R_\rho$ when l^2 takes on the equilibrium value

$$l_e^2 = \frac{1-\tau R_\rho}{\tau R_\rho}. \tag{2.22}$$

Since the right-hand side is $O(1)$, the lengthscale is that of a buoyancy-layer thickness, $(\mu\kappa_T/g\alpha T_z)^{\frac{1}{2}}$.

The growth rate is maximum at $F_r^2 = \tau R_\rho$ and becomes

$$\lambda_m = \frac{(1-\tau R_\rho)^2}{R_\rho(1-\tau)}, \tag{2.23}$$

with corresponding wavelength (referred to as optimum width in §5)

$$l_m^2 = \frac{1-(\tau R_\rho)^{\frac{1}{2}}}{1-\tau}\left[\frac{1}{(\tau R_\rho)^{\frac{1}{2}}} - \frac{1}{R_\rho}\right]. \tag{2.24}$$

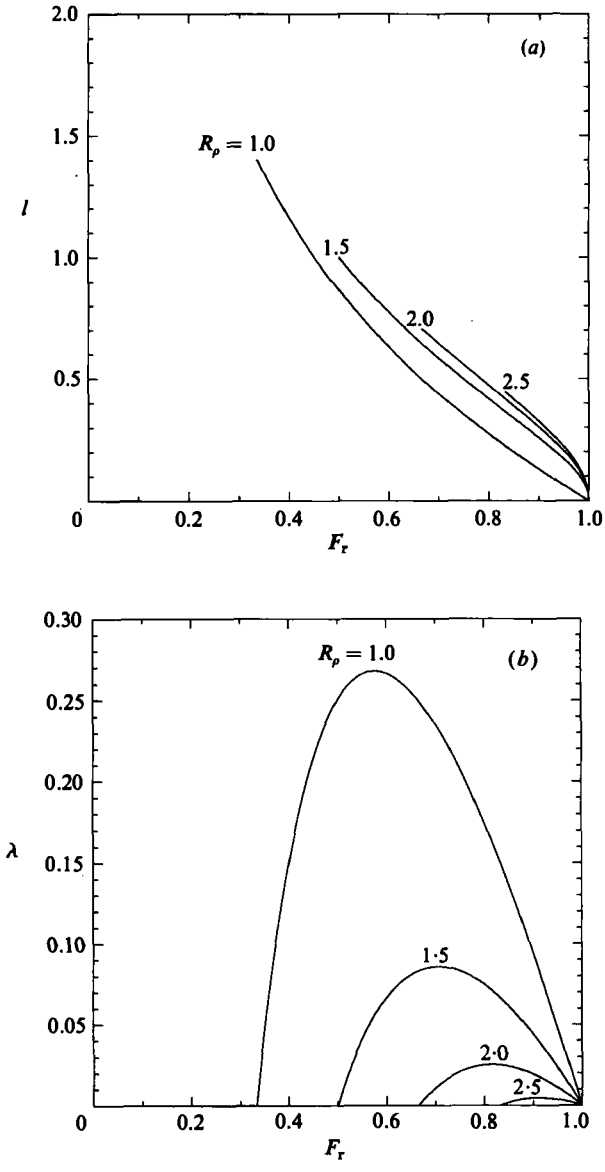

FIGURE 2. (*a*) Wavelength and (*b*) maximum growth rate *vs.* F_r for four values of R_ρ for sugar–salt fingers in the range of F_r for which instability occurs.

There is an infinite amount of potential energy in the unstable gradient $\overline{S}_z$ for a vertically infinite system so that even though there is an equilibrium wavelength given by (2.22), wider fingers can grow exponentially with time. The foregoing results are valid for the parameter ranges

$$1 \leqslant R_\rho \leqslant \tau^{-1}, \quad \tau R_\rho \leqslant F_r \leqslant 1. \tag{2.25}$$

Figure 1 shows l_e, l_m and λ *vs.* R_ρ for $\tau = \frac{1}{3}$, the value appropriate to the sugar–salt experiment. Plots of l_m *vs.* F_r and of λ *vs.* F_r are exhibited in figures 2(*a* and *b*) respectively for a few values of R_ρ in the parts of the range (2.25) for which $\lambda \geqslant 0$.

3. Stability analysis

The fully developed fingers derived above may be unstable to disturbances that depend on the vertical coordinate. The stability problem formulated below is based on the assumption that the basic finger solution does not change appreciably in the time that it takes for a disturbance to grow, i.e. time variations of the basic state are ignored. Therefore, the stability analysis has significance only if the growth rate of an unstable mode is much larger than the time rate of change of the finger itself.

Introduce the perturbation stream function

$$u = \psi_z, \quad w = -\psi_x \tag{3.1}$$

into the vorticity equation to derive

$$M\nabla^2\psi = -g(\alpha T_x - \beta S_x). \tag{3.2}$$

The linearized conservation equations for the perturbations of T and S are

$$T_t = -T^{\mathrm{b}}_x\psi_z - w^{\mathrm{b}}T_x + \overline{T}_z\psi_x + \kappa_T\nabla^2 T, \tag{3.3}$$

$$S_t = -S^{\mathrm{b}}_x\psi_z - w^{\mathrm{b}}S_x + S_z\psi_x + \kappa_S\nabla^2 S, \tag{3.4}$$

where superscript b corresponds to the basic state of §2, which is periodic in x with wavenumber l. To apply Floquet theory (Ince 1926) the perturbation quantities are expressed as

$$\begin{Bmatrix}\psi\\ T\\ S\end{Bmatrix} = \sum_{n=-N}^{N} \exp\left[p_* t + \mathrm{i}(mz + (k+n)x)\, l_*\right] \begin{Bmatrix}\psi_n\\ \mathrm{i}T_n\\ \mathrm{i}S_n\end{Bmatrix}, \tag{3.5}$$

where $i = \sqrt{-1}$, $\mathrm{i}kl_*$ is the characteristic exponent, and for convenience the coefficients T_n and S_n are multiplied by i. The summation is truncated to $2N+1$ terms (see below). Substituting

$$(w^{\mathrm{b}}, T^{\mathrm{b}}, S^{\mathrm{b}}) = (\hat{w}, -\hat{T}, -\hat{S}) \sin l_* x, \tag{3.6}$$

and (3.5) into (3.3) and (3.4) leads to a dispersion relation in the form of a matrix system with $-N \leqslant j \leqslant N$:

$$\begin{aligned} pT_j = &-\left[\frac{(k+j)^2}{K_0^2} + \frac{K_0^2}{R_T}\right] T_j + \frac{(k+j)^2}{K_0^2} S_j + \tfrac{1}{2}m\overline{w}\left\{\left[\frac{1}{R_T} - \frac{k+j+1}{K_1^2}\right] T_{j+1}\right. \\ &\left. -\left[\frac{1}{R_T} + \frac{k+j-1}{K_{-1}^2}\right] T_{j-1} + \frac{k+j+1}{K_1^2} S_{j+1} + \frac{k+j-1}{K_{-1}^2} S_{j-1}\right\}, \end{aligned} \tag{3.7}$$

$$\begin{aligned} pS_j = &-\frac{1}{R_\rho}\frac{(k+j)^2}{K_0^2} T_j + \left[\frac{1}{R_\rho}\frac{(k+j)^2}{K_0^2} - \frac{\tau K_0^2}{R_T}\right] S_j + \tfrac{1}{2}m\overline{w}\left\{\left[\frac{1}{R_T} + \frac{1}{\tau R_\rho}\frac{k+j+1}{K_1^2}\right] S_{j+1}\right. \\ &\left. + \left[-\frac{1}{R_T} + \frac{1}{\tau R_\rho}\frac{k+j-1}{K_{-1}^2}\right] S_{j-1} - \frac{1}{\tau R_\rho}\frac{k+j+1}{K_1^2} T_{j+1} - \frac{1}{\tau R_\rho}\frac{k+j-1}{K_{-1}^2} T_{j-1}\right\}, \end{aligned} \tag{3.8}$$

where the stream function has been replaced by its value from the vorticity equation

$$\psi_j = \frac{g}{\mu l_*}(-\alpha T_j + \beta S_j)\frac{k+j}{K_0^2}. \tag{3.9}$$

The following symbols are used in (3.7)–(3.9):

$$\left.\begin{aligned} K_s^2 &= (k+j+s)^2+m^2, \\ R_T &= \frac{g\alpha\overline{T}_z}{\mu\kappa_T l_*^2}, \\ \overline{w} &= \frac{\hat{w}}{l_*\kappa_T}, \\ p &= \frac{p_*\mu}{g\alpha\overline{T}_z}. \end{aligned}\right\} \tag{3.10}$$

N has been taken large enough so that the real part of the eigenvalue p, corresponding to maximum growth rate, changes by less than 1 % when N is doubled, an accuracy that is achieved with $N = 5$ for fingers of maximum growth rate and $N = 10$ for wider fingers.

4. Stability results

4.1. *Wide fingers*

As described in the Introduction, the Hele-Shaw cell enables one to alter the effect of gravity by inclining the apparatus so that the plates of the cell are at an angle θ with the horizontal plane and g is replaced by $g_r = g\sin\theta$. The non-dimensional wavenumber l_m of fingers with maximum growth rate is still given by (2.24), but the dimensional wavenumber l_* in (2.17) is altered by the factor $(\sin\theta)^{\frac{1}{2}}$. Thus, a small value of θ will lead to a wide finger (small l_*).

Taylor & Veronis (1986) generated fingers in an experiment with a layer of uniform sugar (S) solution above a layer of uniform salt (T) solution with a value of R_ρ ($= \alpha\Delta T/\beta\Delta S$) of 2.0 and with the apparatus inclined 10° from the horizontal. Since the initial gradients, $\overline{T}_z$ and $\overline{S}_z$, were very large, narrow fingers formed. As they penetrated into the reservoirs above and below, they redistributed T and S and reduced the mean gradients. As the system evolved, the width of the fingers increased and after some days an array of long, wide fingers was established. Figure 3(*a*) shows a shadowgraph of a small portion of the system containing fingers with widths of approximately 0.8 cm.

The Hele-Shaw cell was then raised upright; accordingly, effective gravity was increased six-fold and the preferred finger width was decreased to $1/\sqrt{6}$ that of the established pattern. Fingers with the preferred width were generated via a small-scale instability that grew from the boundary region between fingers and penetrated the wide fingers at an angle initially well below 45° (figure 3*b*). Eventually, the ends of these disturbances turned toward the vertical (which gives the illusion that the angle of penetration is steeper) and joined with similar features above and below to establish a pattern of narrower fingers.

The pattern of wide cells shown in figure 3(*a*) was observed five days after the experiment had been started. By that time the fingers had penetrated to the top and bottom of the Hele-Shaw cell, and since no measurements of the mean gradients, $\overline{T}_z$ and $\overline{S}_z$, were made, the appropriate value of R_ρ is not known. The stability calculation is based on the initial reservoir concentrations which give $R_\rho = 2$.

The instability is explored using a model with an initial pattern of wide fingers corresponding to $g\sin(10°)$. For the perturbation the full value of gravity is used (consistent with fingers of width $1/\sqrt{6}$ that of the initial pattern), i.e. the model

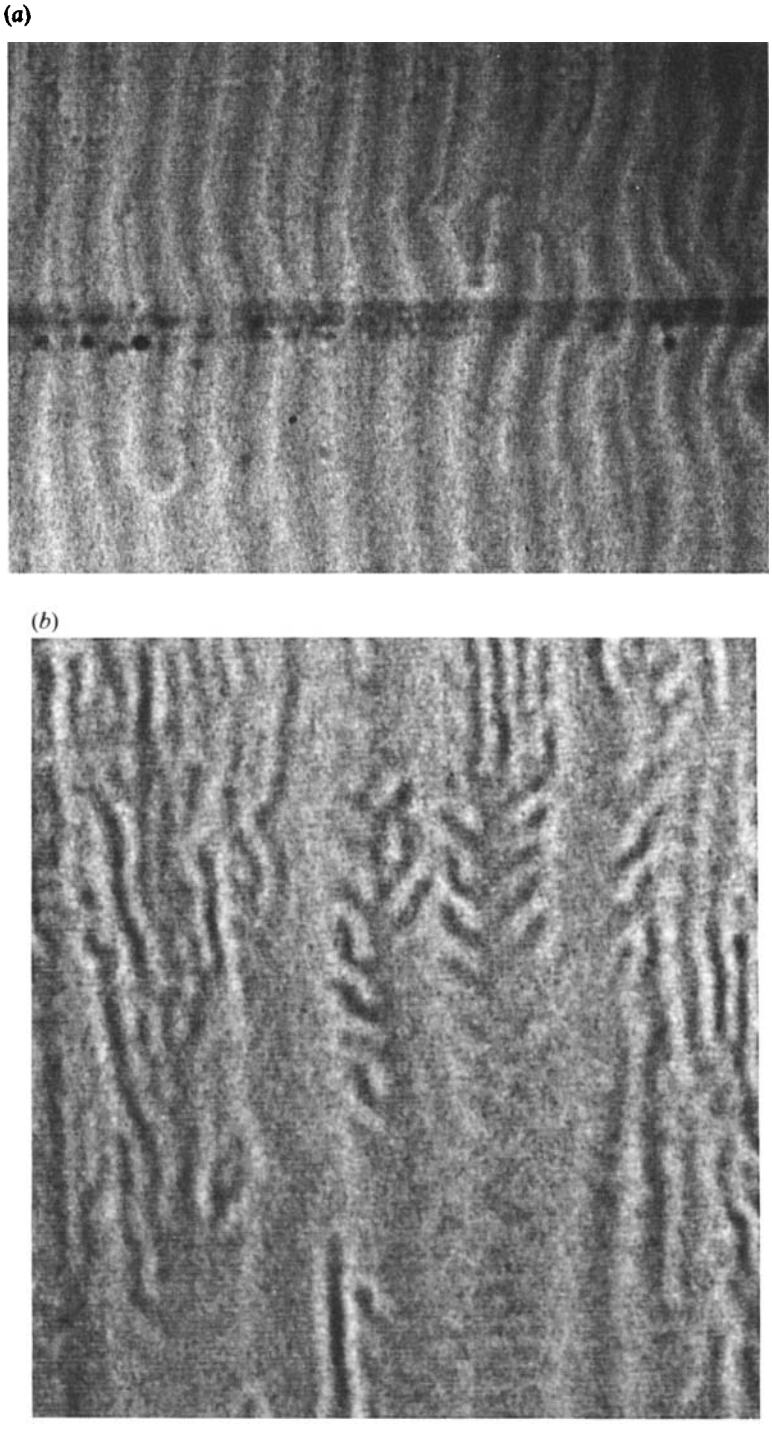

FIGURE 3. (*a*) Sugar–salt fingers that have evolved from an initial two-layer configuration in a Hele-Shaw cell inclined 10° from horizontal. Fingers on the right show disturbance caused by penetration of wider fingers from reservoirs above and below. (*b*) Slanted instability that occurs when wide fingers of figure (*a*) are subjected to stronger gravity by raising tank upright. Dark fluid is salty and less sweet, light fluid contains more sugar and less salt.

matches the experimental conditions. Mathematically, the value of l_* in (3.5) corresponds to the wavenumber of the initial finger pattern, and g in R_T in (3.10) corresponds to $\theta = 90°$. From the definition of l^2 in (2.17) we can write

$$l_*^2 = \frac{g_r \alpha \overline{T}_z}{\mu \kappa_T} l^2 \tag{4.1}$$

where g_r is the reduced value of g for the initial pattern. Then

$$R_T = \frac{g \alpha \overline{T}_z}{\mu \kappa_T l_*^2} = \frac{g}{g_r l^2}. \tag{4.2}$$

Two sets of calculations were made, one with the equilibrium wavenumber l_e^2 for l^2 in (4.2) and the other with the wavenumber of maximum growth rate l_m^2 substituted into (4.2). The remaining parametric values are $\tau = \frac{1}{3}$ and $g/g_r = 6$. In all calculations the most destabilizing perturbations occurred for $k = 0$ and were non-oscillatory. The growth rate was nearly proportional to $\overline{w}$, and $N = 10$ sufficied to give a value correct to 1 %.

Though the details of the calculations differ with different parametric values, the most important result, viz. that wide cells are unstable, is independent of the specific values used. For that reason we give results only for the most unstable perturbations and then discuss the results in terms of physical processes that are consistent with the observed (and calculated) behaviour. The more general stability problem is discussed in §4.2.

The first stability calculation was carried out with l_e^2 for l^2 in (4.2) and with $\overline{w} = 10$. The instability with maximum growth rate gives $p = 1.68$ and occurs for $k = 0$ and $m = 1.74$. The second was based on l_m^2 for l^2 in (4.2) and with $\overline{w} = 10$. The most unstable mode has $k = 0$, $m = 4.15$ and the growth rate is $p = 2.27$. For the present set of parameters but with $m = 0$ convection by the fingers has no effect and the system reduces to the problem of the previous section where the maximum growth rate (figure 1) is $\lambda_m = 0.024$. Since p is much larger than λ_m, the basic finger pattern can be considered quasi-steady and the present stability analysis is pertinent.

The instabilities for the two sets of calculations are qualitatively the same. With l_m^2 as the basic wavenumber two modes, one symmetric, the other antisymmetric with respect to a finger boundary, have nearly the same growth rate though the antisymmetric one grows marginally faster. A plot of the density field encompassing two rising and two sinking fingers and four cycles in z is shown in figure 4 (*a*) for the antisymmetric mode and in figure 4 (*b*) for the symmetric mode. The amplitude of the perturbation was chosen to be the same as that of the density variation of the wide fingers. The effect of the mean gradients is not included. The light and dark regions correspond to those of figure 3 (*b*). (In figure 4 the boundary between light (less salty, sweet) and dark (salty, less sweet) fluid is where the perturbation density vanishes. In the experiment light and dark are based on the refractive index of the fluid and the division is not at all as sharp.) Although the two modes have nearly the same growth rate, only the antisymmetric mode is observed experimentally (figure 3*b*).

With l_e^2 for the basic wavenumber the antisymmetric mode is definitely the more unstable. In this case the initial finger is narrower and the antisymmetric mode admits an interpenetration of alternate disturbances into the middle of each finger whereas the symmetric perturbations bump heads. Therefore, the latter are less effective in redistributing the stabilizing property (see below). Since l_m corresponds to a wider basic finger the perturbation near each finger boundary is less affected by

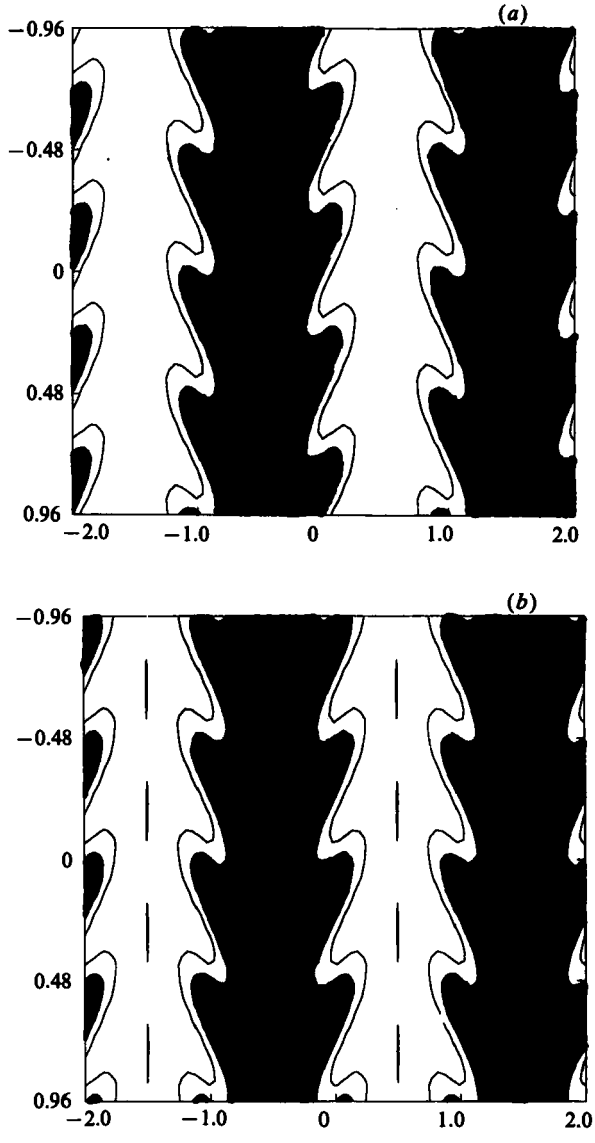

FIGURE 4. Unstable perturbation on long, wide fingers. Amplitude of density perturbation taken equal to that of basic fingers. (*a*) Antisymmetric mode; (*b*) symmetric mode.

the disturbances from the finger boundaries to the right and left so the growth rates of the symmetric and antisymmetric modes are more nearly the same, as mentioned above.

A tentative physical explanation of the instability was included in the paper by Taylor & Veronis (1986). Initially the salt and sugar distributions very sinusoidally in the horizontal. When the Hele-Shaw cell is brought upright, the value of g is increased and the buoyancy-layer thickness is decreased. Since the salt adjustment across the boundary of a rising and a sinking finger takes place on the scale of a buoyancy layer, the salt distribution will be relatively uniform near the middle of each cell. A perturbation with a vertical lengthscale of the order of the buoyancy layer

R_ρ	m	p	λ_m (equation (2.23))	F_e
1.5	0.90	2.18	0.086	0.707
2.0	0.85	1.05	0.025	0.82
2.5	0.93	0.532	0.0046	0.91

TABLE 1. Vertical wavenumber and growth rate of the most unstable perturbation for $w = 10, \tau = \frac{1}{3}$ and three values of R_ρ. Last two columns give λ_m and F_r for basic fingers.

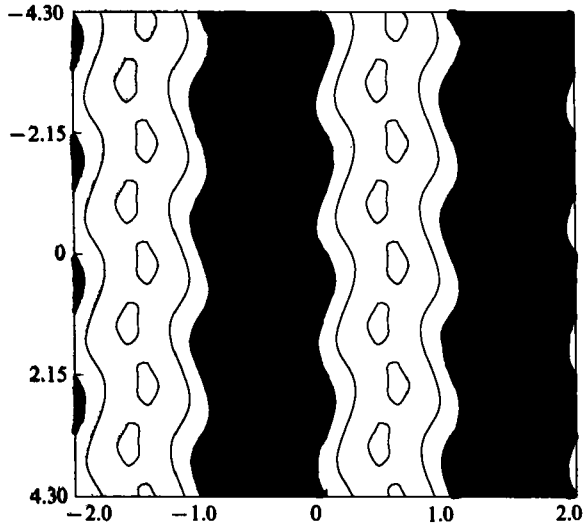

FIGURE 5. Same as figure 4(a) but wavelength of basic fingers corresponds to maximum growth rate in unperturbed state. Antisymmetric mode only.

can penetrate into the uniform salinity region near the centre of the finger and lose its salt anomaly by diffusion. However, the sugar anomaly remains, since $\kappa_S < \kappa_T$. Thus, less-sweet water (the dark tongues) will penetrate upward into the sweet, less-salty light regions and sweeter water (light tongues) will penetrate downward into the salty, less-sweet dark regions.

The results of the calculations are consistent with the physical mechanism that is proposed. The narrower cells associated with l_e rather than l_m become unstable to a mode with $m = 1.74$ since the buoyancy-layer scale is a larger proportion of the finger width. In calculations with $g/g_r = 10$ the basic finger is wider, the buoyancy scale is relatively smaller and the most unstable mode has $m = 6.3$. As expected, the slope of the inclined perturbations decreases (m increases) as the basic finger width increases.

Holyer (1983) obtained horizontally penetrating instabilities for a fluid with (density) compensating horizontal gradients of salt and heat superposed on vertical gradients. For a situation analogous to the present one with salt fingers, she found that cold fresh fluid penetrated horizontally up into warm salty fluid and vice versa, just as we have described here. The same physical mechanisms are present in the two systems even though the specific configurations differ. Hence, both systems lead to horizontal interleaving.

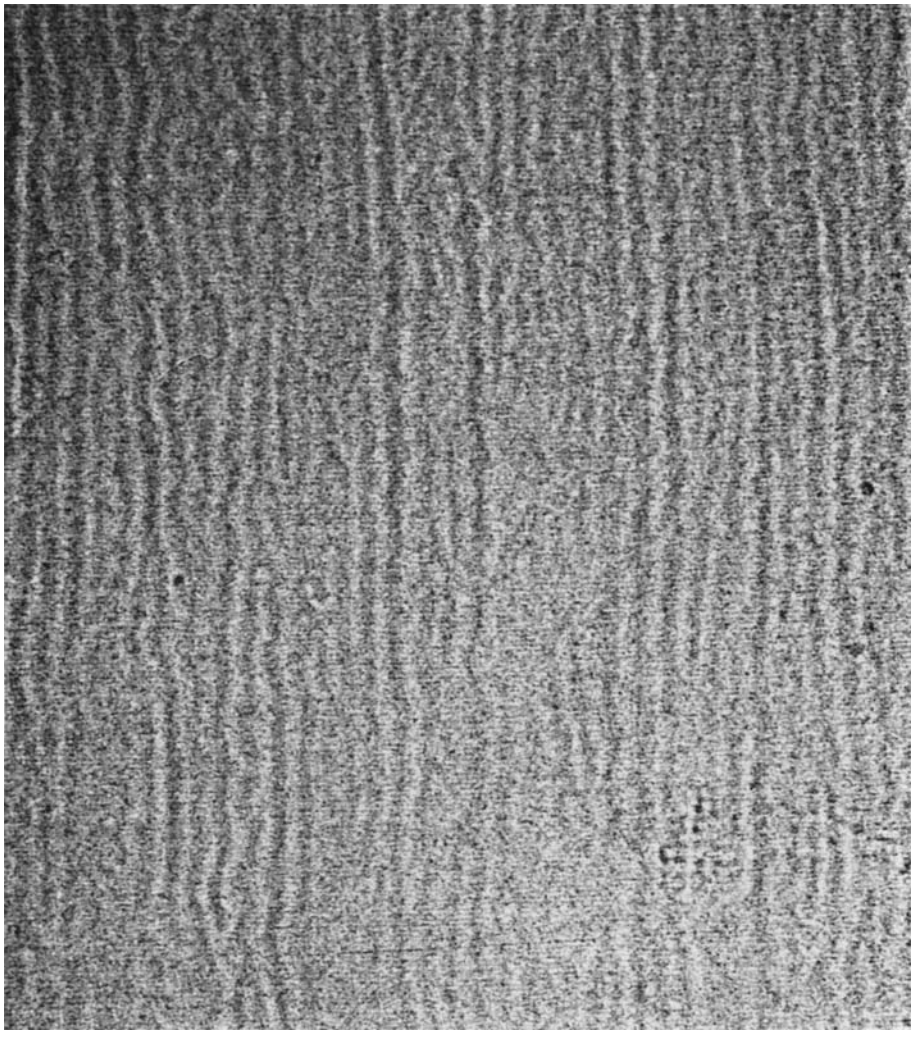

FIGURE 6. Long wiggly fingers in a Hele-Shaw cell exhibit instability obtained from stability analysis. The wiggly structure is enhanced by looking at the figure at an angle from below.

4.2. *Fingers with preferred width*

The stability analysis of most interest is based on fingers corresponding to maximum growth rate in the basic state. If these are unstable, one ought not to observe long straight fingers. The calculation in this case is for $g/g_r = 1.0$. A value of $N = 5$ sufficies to give the growth rate with an error of less than 1 %

In all of the calculations the disturbance with the maximum growth rate was non-oscillatory, antisymmetric about the finger boundary, and was associated with a characteristic exponent (k) of zero. The corresponding values of m and p, along with the values of λ_m and F_r for the basic finger, are listed in table 1 for three different values of R_ρ and with $\overline{w} = 10$. For larger values of $\overline{w}$, m remains nearly the same and p grows proportionately. As $\overline{w}$ becomes very small, the growth rate tends toward the value λ_m.

The most interesting conclusion, of course, is that straight fingers are unstable to perturbations with a vertical variation. In the three calculations reported in table 1 the vertical wavenumber is close to unity. Thus, the instability once again has a vertical scale of the order of the buoyancy-layer thickness (which is the dimensional scaling for the vertical wavenumber).

Figure 5 illustrates the density structure of the most unstable mode for the case with $R_\rho = 2.5$. Once again the perturbation amplitude is the same as the amplitude of the density variation of the basic fingers. The lateral penetration of the perturbation is considerably smaller than it is when the basic fingers are too wide. (The vertical scale in figure 5 is compressed; that of figure 4 is expanded. Thus, the difference in penetration is greater than a comparison of the diagrams would suggest.)

The instability derived here leads to long wiggly fingers. A photograph of an experiment that shows such a structure appears in figure 6. These fingers had grown from an array of wide fingers after the tank had been raised upright from an inclined position. The instability to narrower fingers evolved during the first hour and a pattern of long, nearly straight fingers emerged. The photograph shows the configuration twenty-four hours later. The wavy columns indicate that the non-oscillatory instability derived for fingers of 'optimum' width equilibrates at finite amplitude.

Holyer (1984) concluded that straight, two-dimensional fingers in a regular fluid are unstable to a non-oscillatory disturbance of the same type for the heat–salt case, though her corresponding vertical wavenumber is smaller ($m = 0.30$). For the salt–sugar system she concludes that the most unstable mode is oscillatory with $m = k = 0.5$. Her most unstable non-oscillatory mode grows at about two-thirds that rate. Inertial terms are important in Holyer's analysis, as can be seen from the dependence of her results on the Prandtl number. In the Hele-Shaw system the Prandtl number is effectively infinite.

As in Holyer's calculations there are other unstable modes in addition to the ones reported here. However, the growth rates for those cases are invariably much smaller than the non-oscillatory one with $k = 0$.

4.3. *Narrow fingers*

The same type of instability occurs when the finger width is smaller than that corresponding to maximum growth rate. Experimentally this configuration can be realized by letting the fingers evolve in an upright Hele-Shaw cell and then inclining the apparatus. With $g/g_r = 0.5$, $R_\rho = 2$ and $\overline{w} = 10$ a perturbation with $k = 0$ and $m = 0.4$ grows the fastest ($p = 0.26$). The vertical lengthscale is again about the size of the buoyancy-layer thickness and the lateral penetration is weaker.

5. Discussion

The foregoing analysis of the structure and the stability of fingers is based on the assumption that they are infinitely long. For parts of the analysis that approximation is reasonable. In particular, the conclusion that most fingers are unstable to a perturbation with a vertical scale of the order of the buoyancy-layer thickness is not likely to be altered by treating finite, but very long, fingers. The fact that the instability is the one with the largest growth rate means that observed quasi-steady salt fingers are very likely to be wiggly rather than straight.

In retrospect, the derived instability is not surprising. The key feature of salt fingers is the buoyancy layer which transports the stabilizing property across the finger boundary from the finger where it hinders instability to the finger where it helps

the instability. Long straight fingers make use of the horizontal transport across the finger wall. The unstable perturbations add vertical structure so that the same physical process can transport the stabilizing property vertically to the adjoining cell across the wave boundary. Evidently, the cost involved in the small horizontal excursion of the fluid (horizontal flow does not tap the potential energy of the system) is more than compensated for by the increased transport of the stabilizing property. Perhaps the most significant quantitative result is that the preferred vertical wavenumber always corresponds to the buoyancy-layer thickness, which, as Howard & Veronis (1987) have shown, maximizes the buoyancy flux. The stabilizing property is redistributed by the buoyancy layer so that the gravitational stability of the overall system is reduced. This physical picture, fortified by the quantitative results of the stability analysis, should help to explain the observed wiggly structure of salt fingers. However, figure 3(*a*) shows that not all salt fingers are wiggly. Observations of the evolving salt-finger zone indicate that the salt fingers of optimum scale are not generated by local horizontal processes but rather by formation of larger scales in the transition region between the finger zone and the boundary reservoirs. These large-scale features then penetrate vertically from the transition region through the finger zone and eventually to the other reservoir. It appears that these penetrating fingers move rather quickly through the fluid (at least for the reservoir differences in the observed experiments) and that the instability derived in this article does not have time to establish itself before its entire supporting structure is displaced by the penetrating feature.

These two contrasting pictures indicate that one cannot talk about the salt-finger phenomenon as if it were a single process. An initial configuration of uniform mean gradients will be susceptible to the instability analysed here. But a finger zone evolving from an initial two-layer state is much more likely to be dominated by vertically penetrating, transient features. This latter phenomenon is almost certainly what one should expect to occur at either the top or the bottom of interleaving water masses in the ocean. Most laboratory experiments are started from some kind of a layered initial state and probably also evolve via transient penetration.

The beginnings of a treatment of fingers of finite height is contained in an article by Howard & Veronis (1987). The approximation of vertically uniform fingers is retained in the zero-order state when $\tau = 0$, and the role of the buoyancy layer is at the core of the analysis. Then a diffusive correction ($\tau > 0$) describes the concentration of the destabilizing property (S) in the vertical direction in each finger. The focus in that study is on the vertical structure required by the horizontal differences between fingers of finite height.

It seems to me that a real understanding of the salt-finger phenomenon will come only after the role of the transition region is analysed. The really important problem is the transient evolution of the system rather than the stability of a quasi-steady state. It is a difficult problem because both horizontal and vertical processes must be taken into account and the analysis must involve the very different physics of the finger zone and of the reservoirs.

Support from NSF Grant OCE8410154 is gratefully acknowledged. Will Morrell wrote the program and produced the computer graphs. This research was started during a visit to the Research School of Earth Sciences at the Australian National University in Canberra.

REFERENCES

HOLYER, J. 1981 On the collective instability of salt fingers. *J. Fluid Mech.* **110**, 95.

HOLYER, J. 1983 Double-diffusive interleaving due to horizontal gradients. *J. Fluid Mech.* **137**, 347.

HOLYER, J. 1984 The stability of long, steady, two-dimensional salt fingers. *J. Fluid Mech.* **147**, 169.

HOWARD, L. N. & VERONIS, G. 1987 The salt finger zone. *J. Fluid Mech.* (in press).

INCE, E. L. 1926 *Ordinary Differential Equations.* Dover. 558 pp.

SCHMITT, R. W. 1979 The growth rate of supercritical salt fingers. *Deep-Sea Res.* **26A**, 23.

STERN, M. E. 1969 Collective instability of salt fingers. *J. Fluid Mech.* **35**, 209.

TAYLOR, J. & VERONIS, G. 1986 Experiments on salt fingers in a Hele-Shaw cell. *Science* **231**, 39.